International RILEM Conference on Materials, Systems and Structures in Civil Engineering
Conference segment on Service Life of Cement-Based Materials and Structures
22-24 August 2016, Technical University of Denmark, Lyngby, Denmark

COMPUTATIONAL PREDICTION OF RESTRAINT-INDUCED MACROCRACK PATTERNS IN CONCRETE WALLS

Agnieszka Knoppik-Wróbel [(1)], Dirk Schlicke [(2)]

(1) Silesian University of Technology, Gliwice, Poland
(2) Graz University of Technology, Graz, Austria

Abstract
Two independent approaches to predict the restraint-induced macrocrack patterns in walls have been recently proposed by the authors [1, 2]. The model of *Knoppik-Wróbel and Klemczak* [1] is fully numerical whereas the approach of *Schlicke and Tue* [2] is a simplified engineering model on the basis of analytical considerations. Both approaches are macroscopic solutions aiming at a robust prediction of macrocrack patterns with respect to its main driving forces. Both accept a certain level of simplification to ensure a broad applicability, however, their reliability was verified by satisfying results of recalculations of practical observations, as presented e.g. in [4, 6].This contribution presents both approaches and compares the results of each for a given example. Besides computational aspects, mechanical background of the restraint-induced cracking is outlined with special regard to relevant material properties, geometry and restraint situations.

1. Fundamentals on hardening-induced macrocrack formation in walls on foundations

1.1 Driving forces

Concrete is a material which gains its strength and stiffness due to cement hydration. In concrete elements with significant dimensions this leads to remarkable temperature histories, beginning with self-heating due to the heat release of the highly exothermal hydration and limited conductivity of concrete. Subsequently, the hydration reaction rate decreases and the element cools down to the ambient temperature level. In case of walls on foundations, the accompanying temperature deformations are restrained by the rigid connection between both components, which leads in the warming phase to compression in the wall. By cooling down, the imposed compressive stresses are decreased again. However, since also the concrete stiffness evolves strongly at the same time, compressive stresses due to warming are significantly smaller than tensile stresses due to cooling down. Autogenous shrinkage, decreasing viscoelasticity of aging concrete and the difference between concrete temperature

at setting and ambient temperature level increase these tensile stresses additionally. The final resultants of these stresses are a tensile force and a positive bending moment in the cross section of the wall (N_W, M_W) which are superimposed by negative bending moment over the combined cross section of the wall and foundation due to activation of self-weight (M_g). Fig. 1 illustrates this context schematically.

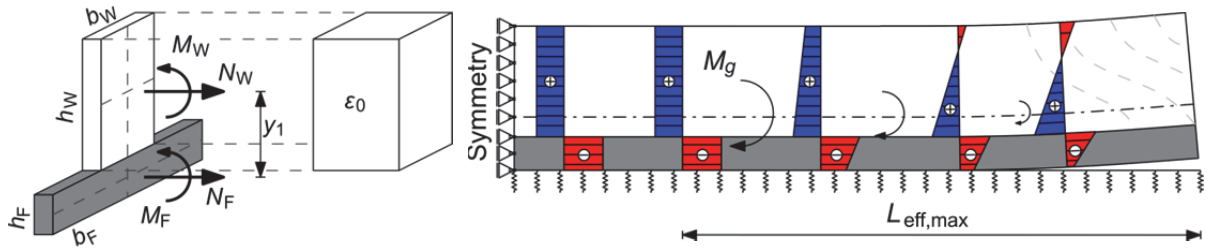

Figure 1. Hardening-induced stress resultants in a wall on a foundation

Besides, transient influences on the temperature and moisture field of the cross section cause internal restraint. Temperature and drying differ significantly between the surface and the interior of the wall, but the accompanying deformations are fully restrained in the uncracked state since the cross section remains plane, which leads to self-balanced stresses or the so-called *Eigenstresses*. For better understanding, Fig. 2 shows the described parts of a hardening-induced stress distribution.

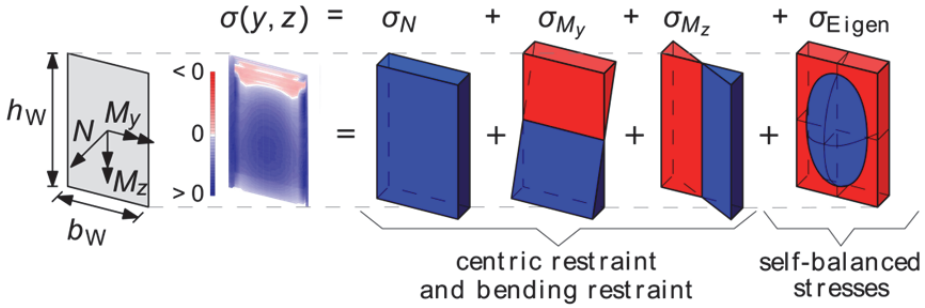

Figure 2. Hardening-induced stress resultants in a wall on a foundation

1.2 Crack formation process

From macroscopic point of view, crack formation starts if the present tensile strength is exceeded in a single material point ($\sigma(y,z) > f_{ct}(y,z)$). As long as Eigenstresses are predominant in this stage, only microcracking – respectively small, locally restricted cracks – occur. However, this type of cracking comes along with softening of the cross-section and beneficial compressive Eigenstresses decrease. In the worst case, only stresses due to stress resultants remain. If these stresses reach the tensile strength of the cross-section, macrocracking is to be expected ($\sigma_N + \sigma_{My} + \sigma_{Mz} > f_{ctm}$). Figure 4 in [3] illustrates this context.

The risk of macrocracking is usually reduced by Eigenstresses, however, as soon as microcracking occurs, the risk of macrocracking increases. This effect is intensified by further Eigenstresses over the width, which are not illustrated in Fig. 2 for clearness reasons.

With respect to the final stress distribution without Eigenstresses as shown in Fig. 1 (right), the formation of macrocracks starts theoretically in the bottom part of the wall. But in these

parts the stiffness of the foundation will reduce the crack width considerably. Only if the macrocrack proceeds over the height of the wall, they become visible. For an efficient design it is very desirable to know whether these macrocracks will stop at a certain height or proceed over the whole wall as well as what is the distance to the next macrocrack. Thus, significant factors influencing these aspects are discussed in the following section.

1.3 Relevant influences on the final macrocrack pattern

The material, technological and environmental conditions determine mostly the magnitude of strains and strain rate, and as such define whether the cracks form or not. The final pattern of cracks depends mostly on geometry, dimensions and restraint conditions.

In general, the maximum tensile stresses in a base-restrained element occur in the plane of symmetry in length direction. This is also where first cracks are formed and where they reach the greatest heights. For the same material, technological and environmental conditions the height of this crack would depend solely on the restraint situation dependent on the *EA* and *EI* as well as *L*/*H* ratios.

Depending on the cracking potential of hardening concrete and geometrical characteristics of the wall, further primary cracks can successively develop in the wall. In shorter walls, these cracks reach lower heights due to a smaller effective *L*/*H* ratio. The cracks are usually vertical in the central part of the wall and slanted near the edges where the rotational restraint becomes more significant. Horizontal cracks can be formed at the joint if shear stresses at the joint exceed the bond strength. A comprehensive description of cracking pattern in walls on foundations is presented in chapter 2 of [4].

1.4 Modelling

The modelling of hardening-induced macrocrack patterns of walls on foundations is a complex matter. The major challenge is to combine complex time- and stress-dependent material behaviour with crack formation on structural level. Only a modest number of contributions exist, whereby the fundamental work by *Rostasy and Henning* [5] is certainly to be seen as one of the most important ones. Next to this, the authors of this paper proposed two approaches independently of each other. Other pertinent proposals are not known.

2. Numerical prediction of hardening-induced macrocrack formation in walls

2.1 Model used

The model used was based on the proposal of *Knoppik-Wróbel and Klemczak* [1]. Calculations were performed with a computer implementation of this phenomenological model that allows for thermo–mechanical analysis of walls on foundation taking into account the effect of hydration heat, temperature development, ageing, creep, soil–structure interaction and behaviour of concrete after damage.

The analysis was performed in two steps. In the first step non-linear and non-stationary thermal fields were determined in concrete elements and subsoil, respectively:

$$c_b \rho \dot{T} = \mathrm{div}(\lambda \,\mathrm{grad}\, T) + q_v(t, T) \quad (1)$$

$$c_b \rho \dot{T} = \mathrm{div}(\lambda \,\mathrm{grad}\, T) \quad (2)$$

where T is temperature, K; c_b is specific heat, kJ/(kg·K); ρ is density, kg/m^3; λ is thermal conductivity, W/(m·K) and $q_v(t,T)$ is the rate of hydration heat generated per unit volume of concrete, W/m^3. The function of hydration heat time-development was described with the approximation function of equivalent age, t_e:

$$Q(t,T) = Q_{tot} e^{[-a_1 t_e{}^{a_2}]} \tag{3}$$

where Q_{tot} is the total amount of hydration heat, J/g, and a_1, a_2 are calibration coefficients dependent on the type of cement. 3rd type boundary conditions were used. The aim of this study was to investigate mechanical behaviour of the wall, thus physical analysis was limited to thermal analysis. The authors are, however, aware that other influences such as autogenous and drying shrinkage as well as coupling of these phenomena are not less important.
The imposed thermal strains were treated as volumetric strains and they were calculated based on the changes of temperature:

$$\mathrm{d}\boldsymbol{\varepsilon}_n = [\mathrm{d}\varepsilon_{n,x} \quad \mathrm{d}\varepsilon_{n,y} \quad \mathrm{d}\varepsilon_{n,z} \quad 0 \quad 0 \quad 0] \tag{4}$$

$$\mathrm{d}\varepsilon_{n,x} = \mathrm{d}\varepsilon_{n,y} = \mathrm{d}\varepsilon_{n,z} = \alpha_T \, \Delta T \tag{5}$$

where α_T is the coefficient of thermal expansion, 1/K.
Viscoelasto–viscoplastic material model with the modified 3-parameter Willam–Warnke failure criterion (MWW3) was used for hardening concrete following *Klemczak* [7] and elasto–plastic material model with the modified Drucker–Prager failure criterion was used for soil (see [4]). Detailed formulations of these models are given in [1] and [4]. The possibility of crack occurrence was defined with the damage intensity factor (DIF):

$$0 \leq DIF = \frac{\tau_{\mathrm{oct}}}{\tau_{\mathrm{oct}}^{f}} \leq 1 \tag{6}$$

Graphical interpretation of DIF is shown in Fig. 3. When DIF = 1, it is equivalent to formation of a crack in the direction perpendicular to the direction of the principal tensile stress. Smeared cracking pattern was used. When failure is reached, material exhibits softening behaviour. In the model, deviatoric and volumetric softening was applied with hardening and softening laws adopted following *Majewski* [8].

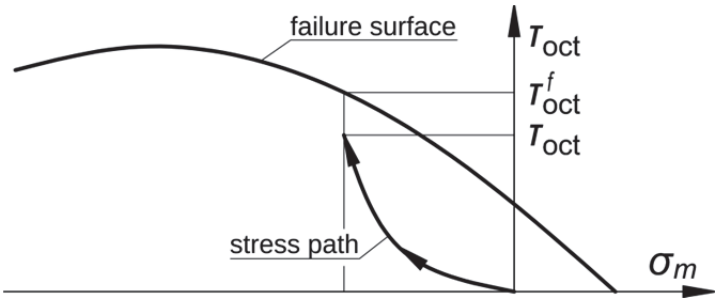

Figure 3. Graphical interpretation of damage intensity factor (*DIF*)

2.2 Reference case and limitations of the model

For the reference case, a wall on foundation was chosen with the dimensions as specified in Fig. 4. Material, environmental and technological data used are given in Tab. 1. The wall was concreted 3 weeks after the foundation. The structure was kept in formwork during the whole analysis. The initial temperature of concrete was T_i = 25°C and the ambient temperature was T_a = 20°C. The initial temperature of soil was equal to the ambient temperature. Final geometry of the wall and input data were chosen after extensive parametric study.

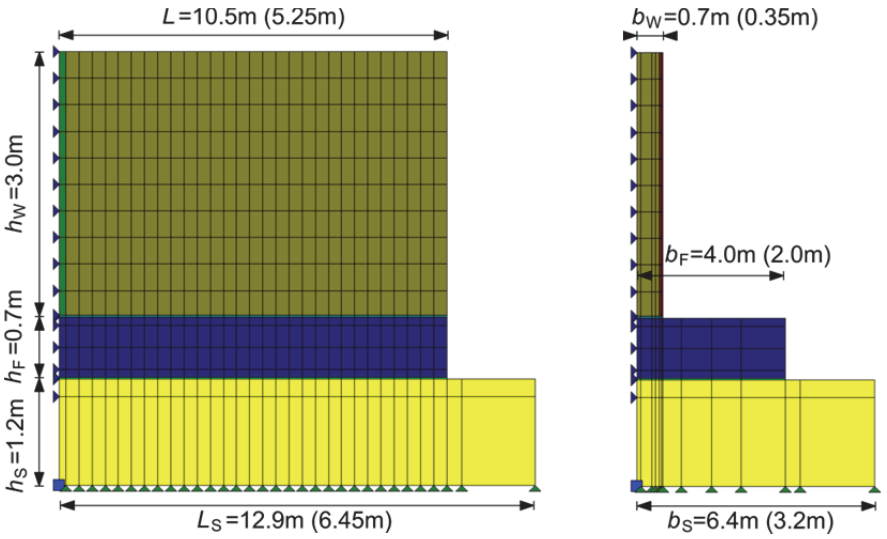

a) longitudinal view *yz* plane, $x = 0$ b) transverse view *xy* plane, $z = 0$

Figure 4. Analysed wall on foundation: geometry and FE mesh for ¼ of wall. Reference case

Table 1: Parameters used in the study.

THERMAL PROPERTIES		
parameter	**unit**	**value**
Thermal conductivity, λ	W/(m·K)	2.6
Specific heat, c_b	kJ/(kg·K)	1.0
Density, ρ	kg/m^3	2500
Amount of cement, C_c	kg/m^3	340
Total heat of hydration, Q_{tot}	J/g	400
Coefficients a_1 and a_2	-	470, -0.1
Coefficient of heat exchange, α_p	W/(m^2·K)	4.0
Thermal expansion coefficient, α_T	1/K	10^{-6}
MECHANICAL PROPERTIES		
parameter	**unit**	**value**
Final value of compressive strength, $f_{c,28}$	MPa	38
Final value of tensile strength, $f_{t,28}$	MPa	2.9
Final value of modulus of elasticity, $E_{c,28}$	MPa	33
Coefficient s for cement	-	0.25
Coefficient n for tensile strength	-	0.6
Coefficient n for modulus of elasticity	-	0.4

During the parameter study some limitations of the model were encountered which needed to be addressed. The following issues should be mentioned:

Finite Element mesh. To capture the most important phenomena, the mesh was densified in the areas of expected damage intensification, i.e. at the joints between the subsequent elements (soil – foundation – wall) and over the width of the wall. Especially a small element size in the core of the wall was needed to realistically simulate the decrease of Eigenstresses during the cracking process. In this regard the model is mesh-dependent, so the same size of finite elements was used in all the analysed models to allow for comparison among them.

Group control of elements. In the model, mechanical properties of hardening concrete (strength, elastic modulus) vary in time according to the assumed ageing functions but, because of computational limitations, the aging of each element could not be simulated independently. To still achieve representative results, groups of elements with comparable aging were defined and mechanical properties assigned according to the mean values of the equivalent age. With respect to the very smooth cooling phase (the wall was continuously kept in the formwork for the whole time), it was adequate to divide the wall only into 4 groups: groups for surface elements (to the depth of 5 cm) and core elements. The elements at the axis of symmetry at the length were also assigned to 2 separate groups to avoid numerical problems at the beginning of cracking. Besides, two additional groups of contact elements were introduced: between the soil and the foundation and between the foundation and the wall. The groups of elements are marked with different colours in Fig. 4.

Cracking. The model assumes smeared cracking, whereby a set of finite elements in which *DIF* reached 1 in tension was considered as cracks. The first crack was always induced in the plane of symmetry by a reduced tensile strength of $0.95 \cdot f_{t,28}$, which ensured the worst-case scenario to happen.

Softening behaviour. If the actual stress state of an element reaches the failure surface, *DIF* reaches the value of 1 and concrete exhibits softening behaviour in this element according to the assumed softening law. Although this softening behaviour can be observed in the results of this study, the extent of this effect seems, from the authors' point of view, to be underestimated. Thus, verification and recalibration of the softening function is required before further investigations.

2.3 Results

Figures 5 and 6 show development of cracks indicated by damage intensity factor (*DIF*) in the reference wall (of 10.5 m length). Areas of expected cracks are marked in red. Figure 5 shows a map of *DIF* right before the primary crack starts to develop in the axis of symmetry of the wall. It can be observed that some locally restricted damage has already developed in the interior of the wall which complies with the before explained influence of Eigenstresses.

Directly after the state of Fig. 5 a primary crack forms in the axis of symmetry between 16 and 18 days. The final state is shown in Fig. 6 and it can be seen that this crack goes through the whole thickness of the wall. The softening behaviour which can be observed in the vicinity of this crack starts directly at the beginning of formation of this crack at 16 days. Moreover, the crack develops from the interior towards the surface of the wall as the wall is kept in the formwork, so any pre-damage on the surface due to temperature shock after early stripping was avoided. The crack reaches on average ~50 % of the height of the wall. As it should be expected from the length-to-height ratio of the wall ($L/H = 3.5$), the crack does not

reach whole height and no further primary cracks are formed. Besides, a horizontally running damage intensity concentration can be observed near the edge of the wall due to shear.

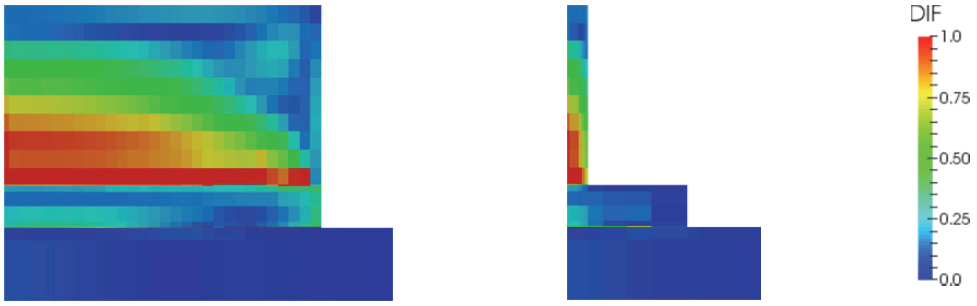

a) *yz*, $x = 0$ (interior) b) *xy*, $z = 0$ (axis of symmetry)

Figure 5. Map of *DIF* in the $L = 10.5$ m wall at the age of wall $t = 15.5$ days

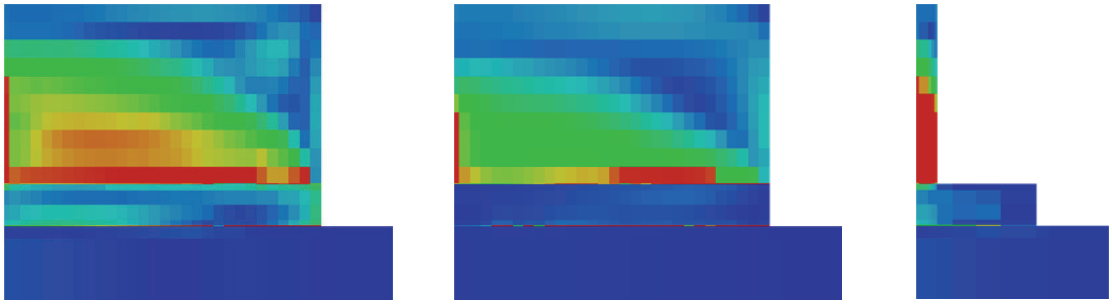

a) *yz*, $x = 0$ (interior) b) *yz*, $x = 0.5\ b_W$ (surface) b) *xy*, $z = 0$

Figure 6. Final map of *DIF* in the $L = 10.5$ m wall at the age of wall $t = 18$ days

Figures 7 to 9 present analogical simulation of damage development in a long wall with the length of 21 m ($L/H = 7$, so twice of the reference case). In Fig. 7 it can be seen again that when the first primary crack develops, softening occurs in its vicinity. It must be noted that the crack in the long wall starts to develop sooner than in the short wall, at the age of wall of 4.5 days. The crack progresses at the thickness of the wall and at its height. It gets its final shape at the age of 8.7 days when it reaches whole height of the wall, which was to be expected for the higher L/H.

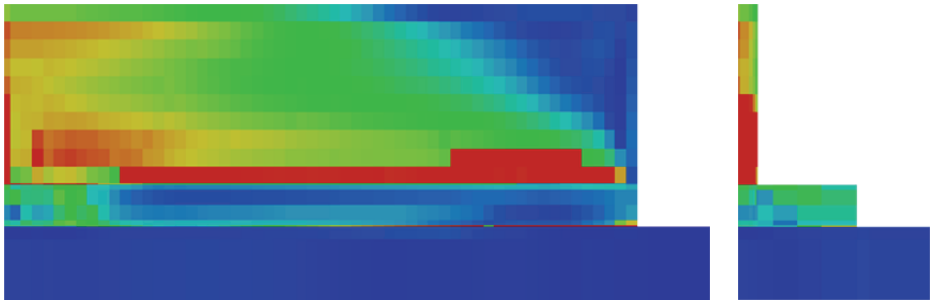

a) *yz*, $x = 0$ (interior) b) *xy*, $z = 0$

Figure 7. Map of *DIF* in the $L = 21$ m wall at the age of wall $t = 5$ days

Figure 8 shows the *DIF* map at the age of 12 days. Intensive damage was indicated in the interior of the wall which represents microcracks due to Eigenstresses. Besides, a fully-

developed separating crack is visible at the surface in the symmetry axis which "splits" the wall in two halves. After the first primary crack, the remaining half of the wall still has an L/H of 3.5 so ongoing cooling forms another primary crack at the age of 12.7 days (Fig. 9).

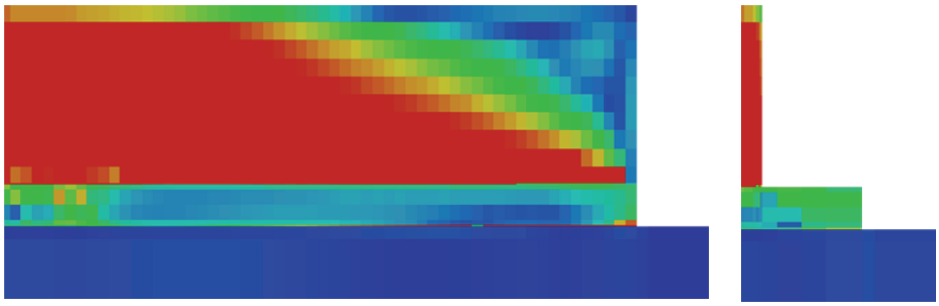

a) *yz*, $x = 0$ (interior) b) *xy*, $z = 0$

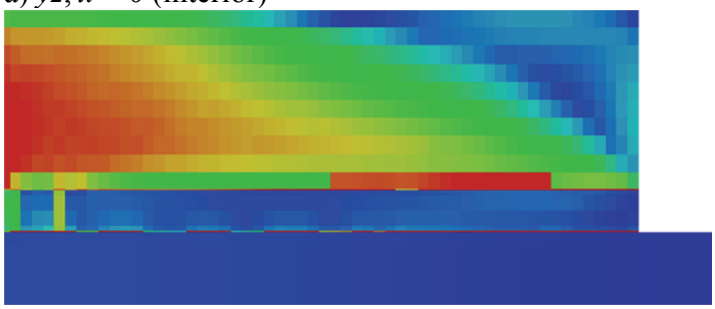

c) *yz*, $x = 0.5\ b_W$ (surface)

Figure 8. Map of *DIF* in the $L = 21$ m wall at the age of wall $t = 12$ days

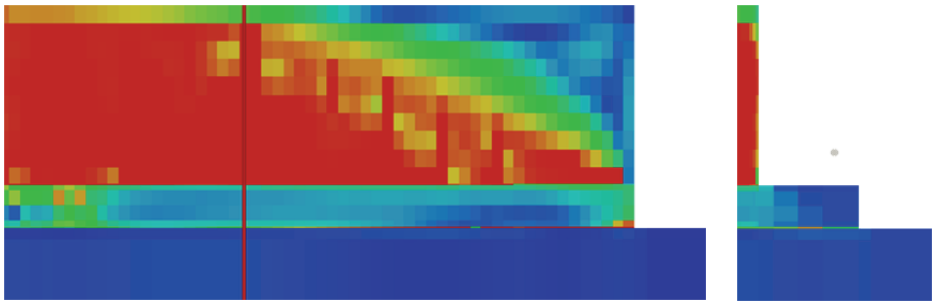

a) *yz*, $x = 0$ (interior) b) *xy*, $z = 4$ m

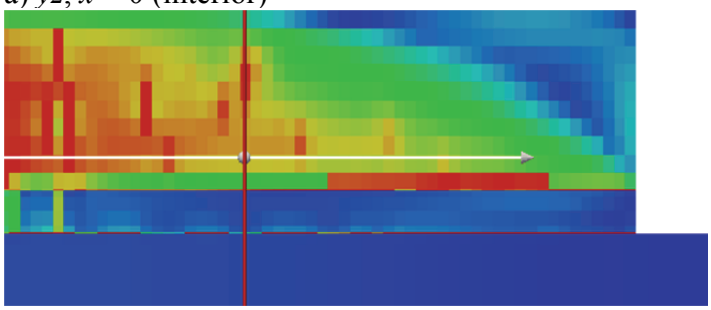

c) *yz*, $x = 0.5\ b_W$ (surface)

Figure 9. Final map of *DIF* in the $L = 21$ m wall

The distance from the axis of symmetry to this crack amounts ~4 m, which is ~$1.3 \cdot h_W$. Softening is observed in the vicinity of this crack, too. In contrast to the corresponding wall of

L/H = 3.5, this crack reaches on average ~80 % of the height of the wall. This difference may result from the fact that the crack is formed earlier, so the strength of the concrete is lower.

3. Analytical prediction of hardening-induced macrocrack formation in walls

The analytical approach to determine the macrocrack pattern of walls on foundations was comprehensively explained by *Schlicke and Tue* in [2]. The basic idea is to relate the distance between primary cracks to the length needed to build up the restraint stresses again. From the theoretical point of view, this length strongly correlates with the height which the primary crack reaches. Thus, the stress at the top of the macrocrack σ_R will be determined according to the remaining concrete area above the top of the crack h_R to compare the resulting curve with the present tensile strength f_{ct}. In all cases where $\sigma_R(h_R)$ falls below the tensile strength, a stop of the cracking will be assumed at this height; in any other case a continuous crack over the wall height will be assumed.

If the crack height is known, the distance between the geometrically set primary cracks will be assumed to have a size of $l_{cr} = 1.2 \cdot h_{cr}$. The application of this approach for the numerically studied systems is shown in Fig. 10. The considered stress resultants were determined fully analytically on the basis of an equivalent deformation impact ε_0 taking into account the temperature field changes due to hydration heat release uniformly distributed in the cross section, stiffness evolution and viscoelasticity for the given material parameters in Tab. 1. Details on the approach used are given by *Schlicke* in [9].

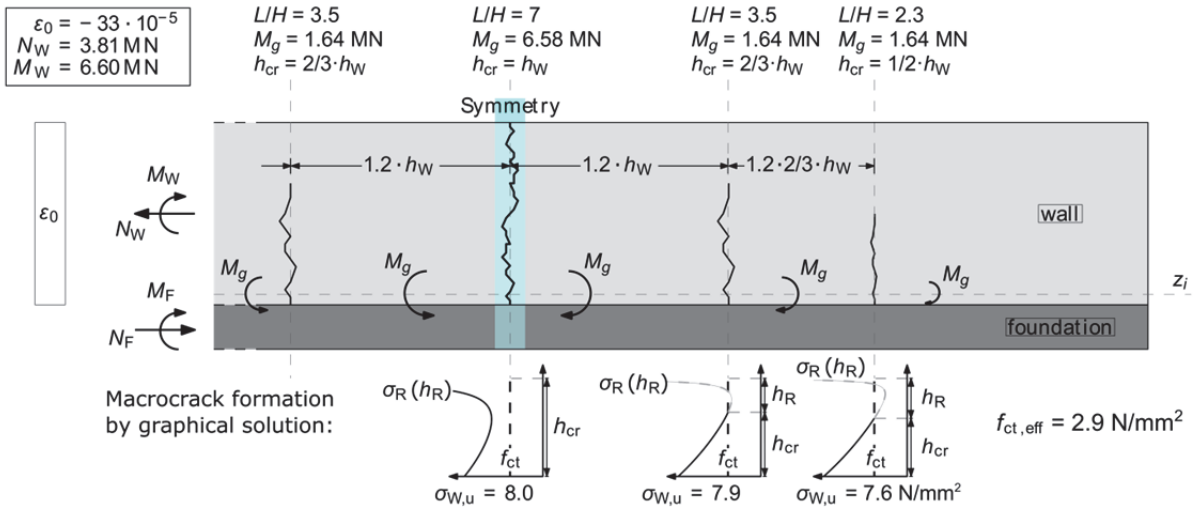

Figure 10. Analytically determined primary crack patterns of the numerically studied cases

4. Discussion and conclusions

The paper presents a comparative study on early-age cracking process with two independent methods recently proposed by the authors [1, 2]. Although the proposed models accept a certain level of simplification, the comparative study gives an acceptable agreement. Both

solutions indicate a separating crack over the whole height in the symmetry axis of the wall with $L/H = 7$ as well as a further stopping crack in the distance of $l_{cr}=(1.25 \pm 0.05) \cdot h_W$ with a height of ~2/3 h_W. A questionable continuation of the analytical approach would indicate another stopping crack at $L/H = 2.3$ with a height of $1/2\,h_W$, but this is unlikely due to the weaknesses of the remaining wall length.

From the authors' point of view the achieved consistency between the numerical and analytical approach confirms the appropriateness of the included simplifications. In detail this refers to the role of Eigenstresses, which are remarkably reduced when any microcracking occurs, so that the process of macrocrack formation is driven predominantly by the stress resultants of the uncracked state AND the conceptual model to derive the distance between the primary cracks from the height reached by the previous crack is adequate. Of course, reinforcement will decrease this distance slightly and cracks which just reached full separation without reinforcement might be stopped somewhat before.

Apart from the comparison between the two models, the insight into the structural behaviour of a wall on a foundation is very valuable for deformation based design concepts as presented by *Schlicke and Tue* in [3] or *Knoppik-Wróbel* in [4].

References

[1] Knoppik-Wróbel, A. and Klemczak B., Degree of restraint concept in analysis of early-age stresses in concrete walls, Engineering Structures 102 (2015), 369-386, DOI: 10.1016/j.engstruct.2015.08.025

[2] Schlicke, D. and Tue, N. V., Minimum reinforcement for crack width control in restrained concrete members considering the deformation compatibility, Structural Concrete 16 (2015), 221-232, DOI: 10.1002/suco.201400058

[3] Schlicke, D. and Tue, N. V., Crack width control – verification of the deformation compatibility vs. covering the cracking force, Proceedings of MSSCE2016/Service Life Segment, Lyngby, Denmark (2016)

[4] Knoppik-Wróbel, A., Analysis of early-age thermal–shrinkage stresses in reinforced concrete walls, PhD thesis, Silesian University of Technology (2015) DOI: 10.13140/RG.2.1.2970.8407

[5] Rostasy, F. S. and Henning, W., Zwang und Rissbildung in Wänden auf Fundamenten, Heft 407. Deutscher Ausschuss für Stahlbeton (1990)

[6] Schlicke, D., Tue, N. V., Klausen, A., Kanstad, T. and Bjøntegaard, Ø., Structural analysis and crack assessment of restrained concrete walls – 3D FEM-simulation and crack assessment, Proceedings of the 1st Concrete Innovation Conference, Oslo, Norway (2014)

[7] Klemczak, B., Adapting of the William–Warnke failure criteria for young concrete, Archives of Civil Engineering 53(2) (2007), 323-339

[8] Majewski, S., MWW3 – elasto–plastic model for concrete, Archives of Civil Engineering 50(1) (2004), 11-43

[9] Schlicke, D., Mindestbewehrung für zwangbeanspruchten Beton, PhD thesis, Graz University of Technology (2014)
http://lamp.tugraz.at/~karl/verlagspdf/buch_schlicke_25052016.pdf